

# Multiple Intelligent Reflecting Surface aided Multi-user Weighted Sum-Rate Maximization using Manifold Optimization

Liyue Zhang<sup>1</sup>, Qing Wang<sup>1</sup>, Haozhi Wang<sup>1</sup>

<sup>1</sup>Tianjin University, Tianjin, China

Email: {zhangliyue, wangq, wanghaozhi}@tju.edu.cn

**Abstract**—Intelligent reflecting surface (IRS) are able to amend radio propagation condition tasks on account of its functional properties in phase shift optimizing. In fact, there exists geometry manifold in the base-station (BS) beamforming matrix and IRS reflection vector. Therefore, we propose a novel double manifold alternating optimization (DMAO) algorithm which makes use of differential geometry theory to improve optimization performance. First, we develop a multi-IRS multi-user system model to maximize the weighted sum-rate, which may lead to the non-convexity in our optimization procedure. Then in order to allocate an optimized coefficients to each BS antenna and IRS reflecting element, we present the beamforming matrix and reflection vector using complex sphere manifold and complex oblique manifold, respectively, which integrates the inner geometry structure and the constrains. By an innovative alternative iteration method, the system gradually converges an optimized stable state, which is associating with the maximized sum-rate. Furthermore, we quantize the IRS reflection coefficient considering the practical constrains. Experimental results demonstrated that our approach significantly outperforms the conventional methods in terms of weighted sum-rate.

**Index Terms**—Intelligent reflecting surface, beamforming, phase-shift optimization, manifolds algorithm

## I. INTRODUCTION

Massive MIMO and millimeter wave will be applied to 5G networks [1]. However, the large-scale antenna arrays and mmWave frequency bands have high power consumption and high hardware cost [2] [3]. IRS is a 2-D planar surface composed of reconfigurable and near-passive reflecting elements with less energy drive, each of them being able to independently adjust the amplitude and phase of the incident signal. This advantage make IRS widely applied to reduce energy consumption and improve the propagation conditions [4] [5]. By optimizing the phase-shift of each IRS reflecting element and the beamforming matrix of the BS according to the perfect CSI, we can reduce the transmit power [6] [7], extend the wireless coverage [3], improve physical layer security [8] [9] and improve the channel capacity [3] [10]-[11].

Considering the channel capacity improving problem, the authors in [10] considered the scenario where there is only one user in wireless communication. In [12], the authors

considered a multi-user scenario and maximized the weighted sum-rate of all users but there is only one IRS in the system. These method only treat one specific scenario. To this end, we aim to model the multi-user multi-IRS optimization problem, which can treat the single-user and single-IRS problem as the special cases.

Recently, iterative optimization methods have been successfully applied in IRS capacity improving problem, such as local search and cross-entropy based algorithm [11]. These methods usually make use greedy search with high computational complexity. Author in [3] transform the problem into convexity case, which can not be extended to more general problem. Thus, we are motivated to explore non-convexity optimization methods to maximize the overall weighted sum-rate with low computational complexity.

**Why manifold optimization:** Recent years we have witnessed the great development of Riemannian optimization algorithm in various types of matrix manifolds. In [13], so as to joint design transmit waveform and receive filter for MIMO-STAP radars, the authors constructed the constraint into a smooth and compact manifold to reduce the computational cost. In the IRS-aided MIMO system, the authors in [14] proposed a channel estimation algorithm by leveraging fixed-rank manifold. The authors in [15] used sphere manifold for data detection. Therefore, taking the geometrical structures and the low-dimension feature of the manifold, we can solve the non-convexity problem with high efficiency when the feasible sets have manifold features, especially in high dimensions [16].

In this paper, we propose a double manifold alternating optimization (DMAO) algorithm to maximize the weighted sum-rate in IRS-aided multi-user MISO system with inter-user interference, by optimizing the beamforming matrix of the BS and the reflection coefficient of each IRS element. Specifically, we use the structural information of the constraint and replace the beamforming matrix and phase-shift vector using complex sphere and complex oblique manifolds, respectively. Via alternatively iteration using geometric conjugate gradient method, we improve the channel capacity significantly.

**Notations:** Scalars are denoted by italic letters, vectors and matrices are denoted by bold-face lower-case and upper-case letters, respectively.  $\mathbb{C}^{n \times p}$  denotes the space of  $n \times p$  complex-valued matrices.  $\text{diag}(\cdot)$  denotes the diagonal operation and

$\text{vec}(\cdot)$  is the inverse operation of  $\text{diag}(\cdot)$ .  $\text{ddiag}(\cdot)$  is a operation that sets all off-diagonal entries of a matrix to zero.  $\mathbb{E}\{\cdot\}$  is the expectation operator.  $\otimes$  is the Kronecker product.  $(\cdot)^*$ ,  $(\cdot)^T$  and  $(\cdot)^H$  denote conjugate, transpose, and conjugate transpose operations, respectively.

## II. SYSTEM MODEL AND PROBLEM FORMULATION

We consider an IRS-aided MISO system as shown in Fig. 1, where the  $K$  users equipped with single receive antenna are served by the BS equipped with  $N$  transmit antennas and the  $S$  IRSs consisted of  $M$  elements. Moreover, We assume that every IRS allocated in the system is exactly the same. What's more, there is an occlusion between the BS and the range of multiple users, so we don't need to consider the channel between the BS and users. The reflection matrix of IRS which is a diagonal matrix composed of the reflection coefficients of all elements is denoted as  $\Phi_s = \text{diag}(\beta_1 e^{j\theta_1}, \beta_2 e^{j\theta_2}, \dots, \beta_M e^{j\theta_M})$ . In addition, we assume that  $\beta_m, m \in (1, 2, \dots, M)$  is always equal to 1 such that only the phase of the reflection coefficient  $\theta_1, \theta_2, \dots, \theta_M \in [0, 2\pi)$  can be adjusted.

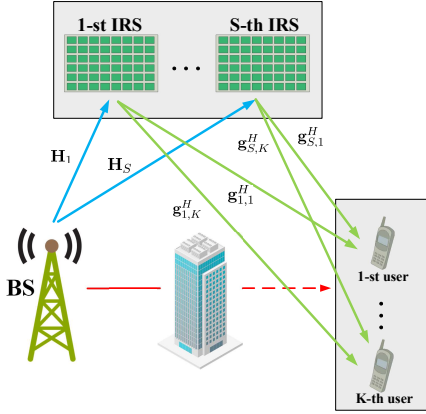


Fig. 1. IRS-aided multiuser MISO system.

The complex transmitted signal from the BS is given by

$$\mathbf{x} = \sum_{k=1}^K \mathbf{v}_k s_k, \quad (1)$$

where  $\mathbf{v}_k$  denotes beamforming vector from the BS to the  $k$ -th user. The transmitted symbols for  $k$ -th user is denoted by  $s_k$ , which satisfies the condition of  $\mathbb{E}\{s_k s_k^H\} = 1$ . Then, the received signal  $y_k$  is expressed as

$$y_k = \left( \sum_{s=1}^S \mathbf{g}_{s,k}^H \Phi_s \mathbf{H}_s \right) \mathbf{x} + u_k, \quad (2)$$

where  $\mathbf{H}_s \in \mathbb{C}^{M \times N}$  denotes the channel between the BS and the  $s$ -th IRS,  $\mathbf{g}_{s,k}^H \in \mathbb{C}^{1 \times M}$  denotes the channel between the  $s$ -th IRS and the  $k$ -th user and  $u_k$  is the received noise for  $k$ -th user which follows the additive white Gaussian noise (AWGN) distribution of  $\mathcal{CN} \sim (0, \sigma_k^2)$ .

In this paper, by employing the classic Saleh-Valenzuela channel model [17], we express  $\mathbf{H}_s$  and  $\mathbf{g}_{s,k}^H$  as

$$\mathbf{H}_s = \sqrt{\frac{NM}{\varrho_{\text{BI}}}} \sum_{l=0}^L \alpha_l \mathbf{a}_{\text{IRS}}(\phi_l^T, \varphi_l^T) \mathbf{a}_{\text{BS}}(\phi_l^T, \varphi_l^T)^H, \quad (3)$$

and

$$\mathbf{g}_{s,k}^H = \sqrt{\frac{M}{\varrho_{\text{IU}}}} \sum_{l=0}^L \alpha_l \mathbf{a}_{\text{IRS}}(\phi_l^T, \varphi_l^T)^H, \quad (4)$$

where  $l = 0$  represents the line-of-sight (LoS) path;  $\mathbf{H}_s$  and  $\mathbf{g}_{s,k}^H$  has  $L$  NLoS paths;  $\varrho_{\text{BI}}$ ,  $\varrho_{\text{IU}}$  denote the path-loss and  $\alpha_l$  is the complex gain of the  $l$ -th path. Here, the azimuth and elevation angles at receiver are denoted by  $\phi_l^T, \varphi_l^T$ , and the azimuth and elevation angles at transmitter are denoted by  $\phi_l^t, \varphi_l^t$ . In (3) and (4),  $\mathbf{a}_{\text{IRS}}(\phi, \varphi)$  and  $\mathbf{a}_{\text{BS}}(\phi, \varphi)$  both satisfy this structure

$$\begin{aligned} \mathbf{a}(\phi, \varphi) &= \frac{1}{\sqrt{RC}} \\ &\times \left[ e^{j \frac{2\pi}{\lambda} d (0 \sin(\phi) \sin(\varphi))}, \dots, e^{j \frac{2\pi}{\lambda} d ((R-1) \sin(\phi) \sin(\varphi))} \right]^T \\ &\otimes \left[ e^{j \frac{2\pi}{\lambda} d (0 \cos(\varphi))}, \dots, e^{j \frac{2\pi}{\lambda} d ((C-1) \cos(\varphi))} \right]^T, \end{aligned} \quad (5)$$

where  $R$  and  $C$  represent the number of antennas in the rows and columns of the antenna array respectively.  $\lambda$  is the wavelength and  $d$  is the distance between adjacent antenna elements which can be assumed to be  $\lambda/2$ .

Therefore, the achievable rate for  $k$ -th user,  $k = 1, \dots, K$ , is

$$\mathcal{R}_k = \log_2(1 + r_k), \quad (6)$$

where

$$r_k = \frac{|\mathbf{g}_k^H \Phi \mathbf{H} \mathbf{v}_k|^2}{\sum_{j \neq k}^K |\mathbf{g}_k^H \Phi \mathbf{H} \mathbf{v}_j|^2 + \sigma_k^2}, \quad (7)$$

with  $\mathbf{g}_k^H = [\mathbf{g}_{1,k}^H, \mathbf{g}_{2,k}^H, \dots, \mathbf{g}_{S,k}^H]$ ,  $\mathbf{H} = [\mathbf{H}_1^T, \mathbf{H}_2^T, \dots, \mathbf{H}_S^T]^T$ , and  $\Phi = \text{diag}(\Phi_1, \Phi_2, \dots, \Phi_S)$ .

We assume that all IRSs have the same type. Therefore, the weight sum-rate maximization optimization problem (P1) for multi-user can be formulated as

$$\begin{aligned} (\text{P1}) : \max_{\mathbf{V}, \Phi} f_1(\mathbf{V}, \Phi) &= \sum_{k=1}^K \omega_k \mathcal{R}_k \\ \text{s.t. } \text{tr}(\mathbf{V} \mathbf{V}^H) &\leq P, \\ \theta_i &\in \mathcal{F}, i = (1, 2, \dots, SM), \end{aligned} \quad (8)$$

where  $\mathbf{V} = [\mathbf{v}_1, \mathbf{v}_2, \dots, \mathbf{v}_K]$  denotes the beamforming matrix; the weight  $\omega_k$  is the required service priority of the  $k$ -th user and  $P$  is the maximum transmit power at BS;  $\text{tr}(\mathbf{V} \mathbf{V}^H) \leq P$  represents the BS transmit power constraint;  $\mathcal{F}$  denotes the feasible set of the reflection coefficient which has two different assumptions. One is a set of infinite resolution under ideal conditions, and the other is a set of finite resolution controlled by  $Q$ -level quantization order.

### III. MANIFOLD OPTIMIZATION BASED ALGORITHM

In this section, we propose a manifold optimization based algorithm which jointly optimize the beamforming matrix and reflection matrix using manifold optimization to find the optimal solution to problem (P1).

#### A. Reformulate the Problem

To deal with the sum-log problem, we decouple and divide the problem into three sub-problems [18], [19]. By introducing auxiliary variables  $\gamma = [\gamma_1, \gamma_2, \dots, \gamma_K] \in \mathbb{C}^{1 \times K}$ , the original problem (P1) is reformulated as

$$\begin{aligned} \text{(P2)} : \max_{\mathbf{V}, \Phi, \gamma} f_2(\mathbf{V}, \Phi, \gamma) &= \frac{1}{\ln 2} \sum_{k=1}^K \omega_k \ln(1 + \gamma_k) \\ &+ \sum_{k=1}^K \left( -\omega_k \gamma_k + \frac{\omega_k(1 + \gamma_k)r_k}{1 + r_k} \right) \\ \text{s.t. } \text{tr}(\mathbf{V}\mathbf{V}^H) &\leq P, \\ \theta_i \in \mathcal{F}, i &= (1, 2, \dots, SM). \end{aligned} \quad (9)$$

Then we alternatively optimize  $\mathbf{V}$ ,  $\Phi$  and  $\gamma$  jointly. The key idea behind is to fix the other two variables and optimize the remained one until the convergence of the objective function is achieved.

#### B. Fix $\mathbf{V}$ , $\Phi$ and Optimize $\gamma$

During each iteration, the auxiliary variable  $\gamma$  is updated firstly according to  $\mathbf{V}$  and  $\Phi$  at the previous iteration, via setting  $\partial f_2(\mathbf{V}, \Phi, \gamma)/\partial \gamma$  to zero. The updated  $\gamma$  is expressed as

$$\gamma_k = r_k. \quad (10)$$

Observe that  $f_2$  is a concave differentiable function over  $\gamma$  when  $\mathbf{V}$  and  $\Phi$  is held fixed. Substituting (10) back in  $f_2$  recovers the objective function in (8) exactly. This is the reason why (P2) is equal to (P1). In addition, we notice that only one term of the objective function in (P2) is related to  $\mathbf{V}$  and  $\Phi$ . So when optimizing  $\mathbf{V}$  and  $\Phi$ , the objective function can be further simplified as

$$\begin{aligned} \text{(P3)} : \max_{\mathbf{V}, \Phi} f_3(\mathbf{V}, \Phi) &= \sum_{k=1}^K \frac{\omega_k(1 + \gamma_k)r_k}{1 + r_k} \\ &= \sum_{k=1}^K \frac{\omega_k(1 + \gamma_k)|(\mathbf{g}_k^H \Phi \mathbf{H})\mathbf{v}_k|^2}{\sum_{j=1}^K |(\mathbf{g}_k^H \Phi \mathbf{H})\mathbf{v}_j|^2 + \sigma_k^2} \\ \text{s.t. } \text{tr}(\mathbf{V}\mathbf{V}^H) &\leq P, \\ \theta_i \in \mathcal{F}, i &= (1, 2, \dots, SM). \end{aligned} \quad (11)$$

#### C. Fix $\gamma$ , $\Phi$ and Optimize $\mathbf{V}$

Given fixed  $\Phi$ , (P3) is equivalent to

$$\begin{aligned} \text{(P3')} : \max_{\mathbf{V}} f_3(\mathbf{V}) &= \sum_{k=1}^K \frac{\omega_k(1 + \gamma_k)|(\mathbf{g}_k^H \Phi \mathbf{H})\mathbf{v}_k|^2}{\sum_{j=1}^K |(\mathbf{g}_k^H \Phi \mathbf{H})\mathbf{v}_j|^2 + \sigma_k^2} \\ \text{s.t. } \text{tr}(\mathbf{V}\mathbf{V}^H) &\leq P, \end{aligned} \quad (12)$$

Without loss of generality, we normalize the power to get  $\text{tr}(\mathbf{V}\mathbf{V}^H) \leq 1$  and define  $\hat{\mathbf{V}} = [\hat{\mathbf{v}}_1, \hat{\mathbf{v}}_2, \dots, \hat{\mathbf{v}}_K]$  satisfying  $\text{tr}(\hat{\mathbf{V}}\hat{\mathbf{V}}^H) = \text{tr}(\mathbf{V}\mathbf{V}^H) + \|\mathbf{x}\|_2^2 = 1$ , where  $\hat{\mathbf{v}}_k = [\mathbf{v}_k^T, \mathbf{x}_k^T]^T$  and  $\mathbf{x} = [\mathbf{x}_1, \mathbf{x}_2, \dots, \mathbf{x}_K]$  is an auxiliary vector to convert the unequal constraint to be an equal one. As the Frobenius norm is equal to one, we then define a  $(N + 1)K - 1$  dimensional complex sphere manifold  $\mathcal{M}_1 = \{\hat{\mathbf{V}} \in \mathbb{C}^{(N+1) \times K} | \text{tr}(\hat{\mathbf{V}}\hat{\mathbf{V}}^H) = 1\}$ , such that (P3') is equivalent to the unconstrained optimization problem on  $\mathcal{M}_1$ , that is

$$\begin{aligned} \text{(P3'')} : \max_{\hat{\mathbf{V}} \in \mathcal{M}_1} f_3(\hat{\mathbf{V}}) &= \sum_{k=1}^K \frac{\omega_k(1 + \gamma_k)|(\mathbf{g}_k^H \Phi \hat{\mathbf{H}})\hat{\mathbf{v}}_k|^2}{\sum_{j=1}^K |(\mathbf{g}_k^H \Phi \hat{\mathbf{H}})\hat{\mathbf{v}}_j|^2 + \sigma_k^2}, \end{aligned} \quad (13)$$

where  $\hat{\mathbf{H}} = \sqrt{P}[\mathbf{H}, \mathbf{0}]$ .

Now let's review the geometric conjugate gradient(GCG) algorithm [20] for this kind of manifold optimization problem, as given in **Algorithm 1**. For the conjugate gradient algorithm in Euclidean space, the next iteration point can be determined by the step size and search direction. But if the selectable variables define a Riemannian submanifold, it is very likely that the next iteration point isn't on the manifold. Because of this, we need to make different retractions for different manifolds to ensure that the next iteration point is still on the manifold. In **Algorithm 1**, retraction is denoted as  $\mathcal{R}$ . For example, the retraction of  $\alpha_t \eta_t$  ( $\alpha_t$  denotes Armijo step size) at point  $\mathbf{x}_t$  onto the manifold  $\mathcal{M}$  can be expressed as  $\mathcal{R}_{\mathbf{x}_t}(\alpha_t \eta_t)$ . Moreover, if the tangent plane at point  $\mathbf{x}_t$  is defined as  $T\mathcal{M}_{\mathbf{x}_t}$ , then we know that  $\text{Rgrad}\phi(\mathbf{x}_{t+1})$  means the Riemannian gradient at  $\mathbf{x}_{t+1}$  belongs to  $T\mathcal{M}_{\mathbf{x}_{t+1}}$  while  $\eta_t$  means the search direction at  $\mathbf{x}_t$  belongs to  $T\mathcal{M}_{\mathbf{x}_t}$ . Since  $\text{Rgrad}\phi(\mathbf{x}_{t+1})$  and  $\eta_t$  are not in the same tangent plane, they cannot be summed directly. To this end, we need to transport  $\eta_t$  to  $T\mathcal{M}_{\mathbf{x}_{t+1}}$ . In **Algorithm 1**, the operator of vector transport is denoted as  $\mathcal{T}$ . For example, the vector transport of  $\eta_t$  to  $T\mathcal{M}_{\mathbf{x}_{t+1}}$  by combining  $\mathcal{R}_{\mathbf{x}_t}(\alpha_t \eta_t)$  can be expressed as  $\mathcal{T}_{\alpha_t \eta_t}(\eta_t)$ . More **Algorithm 1** details and convergence analysis can be obtained in [20].

As the GCG algorithm make use of first-order information of the cost function, the key step is to calculate the Riemannian gradient of the objective function at the current point. By calculating the Euclidean gradient of the cost function and projecting the Euclidean gradient onto tangent space [21], we have the Riemannian gradient of cost function.

For our problem, we can't use GCG algorithm directly because the variable to be optimized is  $\hat{\mathbf{v}}_1, \dots, \hat{\mathbf{v}}_K$ , which is a certain column of  $\hat{\mathbf{V}}$ , but the constraint is about  $\hat{\mathbf{V}}$ . Therefore, we construct an index matrix which is a  $k$ -order identity matrix  $\mathbf{E}_k$  so that any column of  $\hat{\mathbf{V}}$  can be expressed by  $\hat{\mathbf{V}}$  and the index matrix. If the  $i$ -th column of  $\mathbf{E}_k$  is expressed as  $\mathbf{E}_{ki}$ ,

**Algorithm 1** Geometric Conjugate Gradient Algorithm

**Input:** Retraction  $\mathcal{R}$  on  $\mathcal{M}$  and vector transport  $\mathcal{T}$  on  $\mathcal{M}$ , the cost function  $\phi$ ;

- 1: Initialize point  $\mathbf{x}_0 \in \mathcal{M}$ ;
- 2: Initialize search direction  $\eta_0 = \text{Rgrad}\phi(\mathbf{x}_0)$ ;
- 3: Iteration counter  $t = 0$ ;
- 4: **repeat**
- 5:   Compute  $\alpha_t > 0$  according to ALS Algorithm in [20];
- 6:   Update point  $\mathbf{x}_{t+1} = \mathcal{R}_{\mathbf{x}_t}(\alpha_t \eta_t)$ ;
- 7:   Compute correction parameter  $\beta_{t+1} = \frac{\langle \text{Rgrad}\phi(\mathbf{x}_{t+1}), \text{Rgrad}\phi(\mathbf{x}_{t+1}) \rangle}{\langle \text{Rgrad}\phi(\mathbf{x}_t), \text{Rgrad}\phi(\mathbf{x}_t) \rangle}$ ;
- 8:   Update search direction  $\eta_{t+1} = \text{Rgrad}\phi(\mathbf{x}_{t+1}) + \beta_{t+1} \mathcal{T}_{\alpha_t \eta_t}(\eta_t)$ ;
- 9:    $t = t + 1$ ;
- 10: **until** Convergence;

**Output:** Converged point  $\mathbf{x}_t$ .

then (P3'') is rewritten as

$$(P4) : \max_{\hat{\mathbf{V}} \in \mathcal{M}_1} f_4(\hat{\mathbf{V}}) = \sum_{k=1}^K \frac{\tilde{\gamma}_k |(\mathbf{g}_k^H \hat{\Phi} \hat{\mathbf{H}}) \hat{\mathbf{V}} \mathbf{E}_{kk}|^2}{\sum_{j=1}^K |(\mathbf{g}_k^H \hat{\Phi} \hat{\mathbf{H}}) \hat{\mathbf{V}} \mathbf{E}_{kj}|^2 + \sigma_k^2}, \quad (14)$$

where  $\tilde{\gamma}_k$  is equivalent to  $\omega_k(1 + \gamma_k)$ .

Define  $\tilde{\mathbf{h}}_k^H = \mathbf{g}_k^H \hat{\Phi} \hat{\mathbf{H}}$ , then the Euclidean gradient is simplified to

$$\begin{aligned} \text{Egrad} f_4(\hat{\mathbf{V}}) &= \sum_{k=1}^K \tilde{\gamma}_k \cdot \left( \frac{2\tilde{\mathbf{h}}_k^H \hat{\mathbf{V}} \mathbf{E}_{kk} \tilde{\mathbf{h}}_k \mathbf{E}_{kk}^H}{\sum_{j=1}^K |\tilde{\mathbf{h}}_k^H \hat{\mathbf{V}} \mathbf{E}_{kj}|^2 + \sigma_k^2} \right. \\ &\quad \left. - 2 \sum_{i=1}^K \frac{|\tilde{\mathbf{h}}_k^H \hat{\mathbf{V}} \mathbf{E}_{ki}|^2 \tilde{\mathbf{h}}_k^H \hat{\mathbf{V}} \mathbf{E}_{ki} \tilde{\mathbf{h}}_k \mathbf{E}_{ki}^H}{(\sum_{j=1}^K |\tilde{\mathbf{h}}_k^H \hat{\mathbf{V}} \mathbf{E}_{kj}|^2 + \sigma_k^2)^2} \right). \end{aligned} \quad (15)$$

The projection operator of the tangent plane at point  $\hat{\mathbf{V}}$  on  $\mathcal{M}_1$  is defined as

$$\mathbf{P}_{\hat{\mathbf{V}}}(\Psi) = \Psi - \text{tr}(\hat{\mathbf{V}}^H \Psi) \hat{\mathbf{V}}, \quad (16)$$

where  $\Psi$  represents a matrix in the ambient space.

Then the Riemann gradient can be obtained according to (15) and (16), expressed as

$$\text{Rgrad} f_4(\hat{\mathbf{V}}) = \mathbf{P}_{\hat{\mathbf{V}}}(\text{Egrad} f_4(\hat{\mathbf{V}})). \quad (17)$$

Moreover, the retraction and vector transport on complex sphere are

$$\mathcal{R}_{\hat{\mathbf{V}}_t}(\alpha_t \eta_t)_{\mathcal{SP}} = \frac{\hat{\mathbf{V}}_t + \alpha_t \eta_t}{\|\hat{\mathbf{V}}_t + \alpha_t \eta_t\|}, \quad (18)$$

and

$$\mathcal{T}_{\alpha_t \eta_t}(\eta_t)_{\mathcal{SP}} = \mathbf{P}_{\mathcal{R}_{\hat{\mathbf{V}}_t}(\alpha_t \eta_t)}(\eta_t). \quad (19)$$

The superscript  $(\cdot)_{\mathcal{SP}}$  means that the retraction and vector transport is on the complex sphere manifold.

Finally, we can optimize  $\hat{\mathbf{V}}$  by applying **Algorithm 1** and  $\mathbf{V}$  can be obtained via  $\mathbf{V} = \hat{\mathbf{V}}(1:N, K)$ .

**Algorithm 2** Double Manifold Alternating Optimization Algorithm

**Input:** Channel State Information about  $\mathbf{H}$  and  $\mathbf{g}_1, \mathbf{g}_2, \dots, \mathbf{g}_K$ ; user service priority  $\omega_k$ .

- 1: Initialize  $\hat{\mathbf{V}}$  and  $\mathbf{u}$ ;
- 2: **repeat**
- 3:   Update  $\gamma$  by (10);
- 4:   Update  $\hat{\mathbf{V}}$  to solve (14) using **Algorithm 1**;
- 5:   Update  $\mathbf{u}$  to solve (20) using **Algorithm 1**;
- 6: **until** Convergence;

**Output:** Optimized beamforming vector  $\mathbf{v}_1, \mathbf{v}_2, \dots, \mathbf{v}_K$  for all users; Optimized reflection matrix  $\Phi$ ; Local optimal solution of  $f_1(\mathbf{V}, \Phi)$ .

**D. Fix  $\gamma$ ,  $\mathbf{V}$  and Optimize  $\Phi$** 

In this subsection, we adopt a similar manifold optimization approach to the previous subsection. Define  $\mathbf{u}^* = \text{vec}(\Phi)$ , we have  $\mathbf{u} = (e^{j\theta_1}, e^{j\theta_2}, \dots, e^{j\theta_{SM}})^H$  satisfies  $(\mathbf{u}\mathbf{u}^H)_{ii} = 1, i = 1 : SM$ . Then  $\mathbf{u}$  forms a complex oblique manifold named  $\mathcal{M}_2$ . Naturally, we can derive  $\mathbf{u}^H \text{diag}(\mathbf{g}_k^H) \mathbf{H} = \mathbf{g}_k^H \Phi \mathbf{H}$  and rewrite (P3) as

$$\begin{aligned} (P5) : \max_{\mathbf{u} \in \mathcal{M}_2} f_5(\mathbf{u}) &= \sum_{k=1}^K \frac{\tilde{\gamma}_k |(\mathbf{u}^H \text{diag}(\mathbf{g}_k^H) \mathbf{H}) \mathbf{V}_k|^2}{\sum_{j=1}^K |(\mathbf{u}^H \text{diag}(\mathbf{g}_k^H) \mathbf{H}) \mathbf{V}_j|^2 + \sigma_k^2} \\ \text{s.t. } \theta_i &\in \mathcal{F}, i = (1, 2, \dots, SM). \end{aligned} \quad (20)$$

The projection operator of the tangent plane at point  $\mathbf{u}$  on  $\mathcal{M}_2$  [22] can be characterized by

$$\mathbf{P}_{\mathbf{u}}(\psi) = \psi - \text{ddiag}(\psi \mathbf{u}^H) \mathbf{u}. \quad (21)$$

where  $\psi$  represents a vector in the ambient space.

Then we calculate the Euclidean gradient and the Riemann gradient of  $f_5(\mathbf{u})$  according to (22) at the top of next page and

$$\text{Rgrad} f_5(\mathbf{u}) = \mathbf{P}_{\mathbf{u}}(\text{Egrad} f_5(\mathbf{u})), \quad (23)$$

respectively. Finally, the retraction and vector transport on complex oblique manifold are given by

$$\begin{aligned} \mathcal{R}_{\mathbf{u}_t}(\alpha_t \eta_t)_{\mathcal{OB}} &= \\ \text{ddiag} \left( (\mathbf{u}_t + \alpha_t \eta_t) (\mathbf{u}_t + \alpha_t \eta_t)^H \right)^{-1/2} &(\mathbf{u}_t + \alpha_t \eta_t), \end{aligned} \quad (24)$$

and

$$\mathcal{T}_{\alpha_t \eta_t}(\eta_t)_{\mathcal{OB}} = \mathbf{P}_{\mathcal{R}_{\mathbf{u}_t}(\alpha_t \eta_t)}(\eta_t), \quad (25)$$

where  $(\cdot)_{\mathcal{OB}}$  means the retraction and vector transport on the complex oblique manifold.

The optimization process are summarized in **Algorithm 2**, namely double manifold alternating optimization algorithm (DMAO). Notice that the monotonic property of **Algorithm 2** along with the fact that the objective function is upper-bounded, is sufficient to prove the convergence. Moreover, the computational complexity of **Algorithm 2** is mainly due to

$$\text{Egrad}f_5(\mathbf{u}) = \sum_{k=1}^K \tilde{\gamma}_k \left( \frac{2\mathbf{v}_k^H (\mathbf{H}^H \text{diag}^H(\mathbf{g}_k^H) \mathbf{u}) \text{diag}(\mathbf{g}_k^H) \mathbf{H} \mathbf{v}_k}{\sum_{j=1}^K |(\mathbf{u}^H \text{diag}(\mathbf{g}_k^H) \mathbf{H}) \mathbf{v}_j|^2 + \sigma_k^2} - \sum_{i=1}^K \frac{2|(\mathbf{u}^H \text{diag}(\mathbf{g}_k^H) \mathbf{H}) \mathbf{v}_k|^2 \mathbf{v}_i^H (\mathbf{H}^H \text{diag}^H(\mathbf{g}_k^H) \mathbf{u}) \text{diag}(\mathbf{g}_k^H) \mathbf{H} \mathbf{v}_i}{(\sum_{j=1}^K |(\mathbf{u}^H \text{diag}(\mathbf{g}_k^H) \mathbf{H}) \mathbf{v}_j|^2 + \sigma_k^2)^2} \right). \quad (22)$$

the **Algorithm 1** iterations. Specifically, the calculation of  $\hat{\mathbf{V}}$  requires  $\mathcal{O}(KSM \cdot \max\{SM, N\} + NK^3)$  operations, and solving (20) requires  $\mathcal{O}(S^2M^2NK + SMNK^2 + S^3M^3)$  operations per-iteration of **Algorithm 1**.

#### E. Non-ideal IRS Case

For non-ideal IRS, due to hardware limitations, it is impossible to set the reflection coefficient to an arbitrary value, that is to say, it is impossible to meet the requirement of infinite resolution of the reflection angle. Therefore, in this subsection, the reflection angle is quantified so that it can only be selected from the feasible angle set with the shortest distance from the optimized value. Quantification is realized by

$$\bar{\theta}_i = \underset{\theta' \in \mathcal{F}}{\text{argmin}} |\theta_i - \theta'|, \mathcal{F} = \{0, \frac{2\pi}{Q}, \dots, \frac{2\pi(Q-1)}{Q}\}, \quad (26)$$

where  $\bar{\theta}_i$ ,  $\theta_i$  and  $\theta'$  is the reflection angle of the final output, infinite resolution reflection angle obtained by **Algorithm 2** and feasible angle, respectively.  $\mathcal{F}$  represents the set of feasible angles, which is a set of finite resolution controlled by  $Q$ -level quantization order as mentioned in II.

### IV. SIMULATION RESULTS

Under the framework of the multiuser MISO system in this paper, we assume that all users have single antenna. For BS and all IRSs, the number of antennas in row are fixed and only the number of column antennas can be adjusted. We suppose that the deployed IRSs have the same type. The variance of AWGN for each user is set as  $\sigma_k^2 = -80\text{dBm}$ . The maximum transmit power is set as  $P = 1\text{W}$ . For simplicity, the weight  $\omega_k$  are set to be 1.

$\mathbf{H}_s$  and  $\mathbf{g}_{s,k}^H$ ,  $s = (1, \dots, S)$  and  $k = (1, \dots, K)$ , a total of  $S(K+1)$  channels, all have  $L = 3$  scattering paths with  $\alpha_l \sim \mathcal{CN}(0, 0.4)$ . In addition,  $\alpha_0$  satisfies  $\alpha_0 \sim \mathcal{CN}(0, 2)$ . All azimuth and elevation angles are uniformly distributed in  $[0, 2\pi)$ . The path-loss including  $\varrho_{\text{BI}}$  and  $\varrho_{\text{IU}}$  is given by

$$\varrho = \left( \frac{4\pi f_{\text{carrier}} D}{c} \right)^2, \quad (27)$$

where  $c$  is the speed of light and  $D$  is the distance between two points.  $f_{\text{carrier}}$  is the carrier frequency and is set to 3GHz. We use the Monte Carlo method to simulate the channel realizations under different conditions 500 times in this paper.

We assume a simulation scenario, where the coordinate of the base station is (0, 0), and the coordinates of the two IRSs are (10, 24) and (24, 10), respectively. Users are uniformly distributed in a circular area with a radius of 2 meters, and the center coordinate is (20, 0).

Next, we compare our proposed algorithms with the following four benchmark schemes.

#### 1) Benchmark scheme with random reflection matrix:

The reflection matrix is set randomly. In addition, the beamforming matrix is updated by solving problem (P4).

#### 2) Alternating optimization with maximum ratio transmission (MRT):

The beamforming matrix is set based on the MRT principle as  $\mathbf{V} = \sqrt{\frac{P}{\|\mathbf{H}_{MRT}\|_F^2}} \mathbf{H}_{MRT}^H$ , where  $\mathbf{H}_{MRT}$  is equal to  $\mathbf{g}_k^H \Phi \mathbf{H}$ , while the reflection matrix is updated by solving problem (P5). We optimize the beamforming matrix and the reflection matrix via an alternating manner.

#### 3) Alternating optimization with zero forcing (ZF):

The beamforming matrix is set based on the ZF principle as  $\mathbf{V} = \sqrt{\frac{P}{\text{tr}((\mathbf{H}_{ZF} \mathbf{H}_{ZF}^H)^{-1})}} \mathbf{H}_{ZF}^H (\mathbf{H}_{ZF} \mathbf{H}_{ZF}^H)^{-1}$ , where  $\mathbf{H}_{ZF}$  is

equal to  $\mathbf{g}_k^H \Phi \mathbf{H}$ . On the other hand, the reflection matrix are obtained by solving problem (P5). We also use an alternating manner to optimize the beamforming matrix and the reflection matrix.

4) **Algorithm proposed in [3]:** The beamforming matrix and the reflection matrix are optimized alternately with closed-form expressions, and related auxiliary variables are resolved using Lagrangian multiplier method, bisection search method and CVX toolbox [23].

Let each IRS has  $M = 20$  elements and the number of users is  $K = 4$ , the weighted sum-rate against the BS antennas is shown in Fig. 2. It can be seen that as the number of BS antennas increases, the weighted sum-rate increases monotonically. The reason is that increasing the number of BS antennas can improve the channel conditions, which has been explained in related theories of MIMO. But we also see that the upward trend is getting slower and slower, because the key to determining the weighted sum-rate lies in the transmit power, but the maximum transmit power is set to 1W and has not changed. What's more, for any BS antennas  $N$ , DMAO algorithm we proposed has an overwhelming advantage over other benchmark schemes. It is also observed that the performance achieved by ZF is better than the performance achieved by the algorithm proposed in [3] when  $N$  is large.

In Fig. 3, we plot the weighted sum-rate against the number of reflecting elements where the number of BS antennas is fixed at  $N = 20$  and  $K = 4$ . Note that as the number of elements of IRS grows, the sum-rate also increases. But with the growth of  $M$ , the weighted sum-rate grows slower and slower. On the one hand, the greater the number of reflecting elements, the more incident signal that can be reused. On the other hand, the reflecting elements of IRS is passive elements which can only reuse the incident signal, so there is an upper bound on the improvement of weighted sum-rate. DMAO is also better than other benchmark schemes in this setting.

At last, we simulate scenarios with non-ideal IRS. The

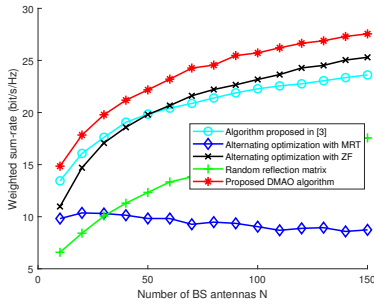


Fig. 2. Weighted sum-rate against the number of BS antennas.

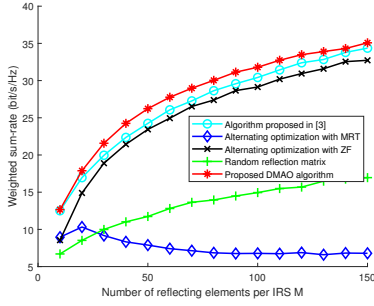


Fig. 3. Weighted sum-rate against the number of reflecting elements per IRS.

parameter is set to  $N, M = 20$  and  $K = 4$ . Fig. 4 shows the performance under different quantifications. As the quantization order  $Q$  increases, the weight sum-rate increases. When  $Q$  approaches infinity, the performance will coincide with the ideal performance. Generally,  $Q$  needs to satisfy  $Q = 2^B$ , which means that the element is controlled by  $B$  bits.

## V. CONCLUSION

In this paper, we proposed the DMAO Algorithm to solve the weighted sum-rate maximization problem in multiuser system by jointly optimizing the beamforming matrix of the BS and reflection coefficient of each IRS element. The utilization of the manifold geometry are proved to be effective. Moreover, we also give an optimization method for the reflection coefficient in the case of non-ideal IRS. The simulation results have demonstrated that the proposed algorithm outperforms

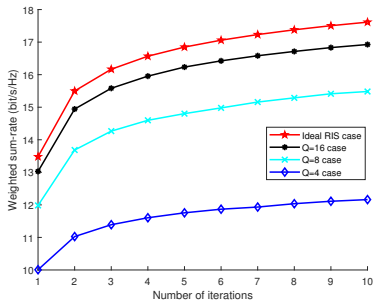


Fig. 4. Weighted sum-rate against quantization order.

benchmark approaches and the system performance has a upper bound with the increase of the number of BS antennas and reflecting elements. It is also shown that the weight sum-rate will rise by increasing the quantization order.

## REFERENCES

- [1] F. Boccardi, R. W. Heath, A. Lozano, T. L. Marzetta, and P. Popovski, "Five disruptive technology directions for 5G," *IEEE communications magazine*, vol. 52, no. 2, pp. 74–80, 2014.
- [2] E. Björnson, Ö. Özdogan, and E. G. Larsson, "Reconfigurable Intelligent Surfaces: Three myths and two critical questions," *IEEE Communications Magazine*, vol. 58, no. 12, pp. 90–96, 2020.
- [3] Y. Cao and T. Lv, "Intelligent Reflecting Surface aided multi-user millimeter-wave communications for coverage enhancement," *arXiv preprint arXiv:1910.02398*, 2019.
- [4] Q. Wu and R. Zhang, "Towards smart and reconfigurable environment: Intelligent Reflecting Surface aided wireless network," *IEEE Communications Magazine*, vol. 58, no. 1, pp. 106–112, 2019.
- [5] E. Björnson and L. Sanguinetti, "Power scaling laws and near-field behaviors of massive MIMO and Intelligent Reflecting Surfaces," *IEEE Open Journal of the Communications Society*, vol. 1, pp. 1306–1324, 2020.
- [6] Y. Li, M. Jiang, Q. Zhang, and J. Qin, "Joint beamforming design in multi-cluster MISO NOMA Intelligent Reflecting Surface-aided downlink communication networks," *arXiv preprint arXiv:1909.06972*, 2019.
- [7] Q. Wu and R. Zhang, "Joint active and passive beamforming optimization for Intelligent Reflecting Surface assisted SWIPT under QoS constraints," *IEEE Journal on Selected Areas in Communications*, 2020.
- [8] M. Cui, G. Zhang, and R. Zhang, "Secure wireless communication via Intelligent Reflecting Surface," *IEEE Wireless Communications Letters*, vol. 8, no. 5, pp. 1410–1414, 2019.
- [9] D. Xu, X. Yu, Y. Sun, D. W. K. Ng, and R. Schober, "Resource allocation for secure IRS-assisted multiuser MISO systems," in *2019 IEEE Globecom Workshops (GC Wkshps)*. IEEE, 2019, pp. 1–6.
- [10] X. Yu, D. Xu, and R. Schober, "MISO wireless communication systems via Intelligent Reflecting Surfaces," in *2019 IEEE/CIC International Conference on Communications in China (ICCC)*. IEEE, 2019, pp. 735–740.
- [11] W. Chen, X. Ma, Z. Li, and N. Kuang, "Sum-rate maximization for Intelligent Reflecting Surface based terahertz communication systems," in *2019 IEEE/CIC International Conference on Communications Workshops in China (ICCC Workshops)*. IEEE, 2019, pp. 153–157.
- [12] H. Guo, Y.-C. Liang, J. Chen, and E. G. Larsson, "Weighted sum-rate optimization for Intelligent Reflecting Surface enhanced wireless networks," *arXiv preprint arXiv:1905.07920*, 2019.
- [13] J. Li, G. Liao, Y. Huang, and A. Nehorai, "Manifold optimization for joint design of MIMO-STAP radars," *IEEE Signal Processing Letters*, 2020.
- [14] T. Lin, X. Yu, Y. Zhu, and R. Schober, "Channel estimation for Intelligent Reflecting Surface-assisted millimeter wave MIMO systems," *arXiv preprint arXiv:2005.04720*, 2020.
- [15] X. Hong, J. Gao, and S. Chen, "Semi-blind joint channel estimation and data detection on sphere manifold for MIMO with high-order QAM signaling," *Journal of the Franklin Institute*, 2020.
- [16] A. Douik and B. Hassibi, "Manifold optimization over the set of doubly stochastic matrices: A second-order geometry," *IEEE Transactions on Signal Processing*, vol. 67, no. 22, pp. 5761–5774, 2019.
- [17] O. El Ayach, S. Rajagopal, S. Abu-Surra, Z. Pi, and R. W. Heath, "Spatially sparse precoding in millimeter wave MIMO systems," *IEEE transactions on wireless communications*, vol. 13, no. 3, pp. 1499–1513, 2014.
- [18] Z. Zhang and L. Dai, "A joint precoding framework for wideband Reconfigurable Intelligent Surface-aided cell-free network," *arXiv preprint arXiv:2002.03744*, 2020.
- [19] K. Shen and W. Yu, "Fractional programming for communication systems—part II: Uplink scheduling via matching," *IEEE Transactions on Signal Processing*, vol. 66, no. 10, pp. 2631–2644, 2018.
- [20] P.-A. Absil, R. Mahony, and R. Sepulchre, *Optimization algorithms on matrix manifolds*. Princeton University Press, 2009.
- [21] N. Boumal, "An introduction to optimization on smooth manifolds," *Available online*, May, 2020.

- [22] J. Hu, X. Liu, Z.-W. Wen, and Y.-X. Yuan, "A brief introduction to manifold optimization," *Journal of the Operations Research Society of China*, vol. 8, no. 2, pp. 199–248, 2020.
- [23] M. Grant and S. Boyd, "CVX: Matlab software for disciplined convex programming, version 2.1," <http://cvxr.com/cvx>, Mar. 2014.